# First-Principles AI Finds Crystallization of Fractional Quantum Hall Liquids

Ahmed Abouelkomsan[*] and Liang Fu[†]
*Department of Physics, Massachusetts Institute of Technology, Cambridge, Massachusetts 02139, USA*

(Received 1 March 2026; accepted 15 July 2026; published 11 August 2026)

When does a fractional quantum Hall (FQH) liquid crystallize? Addressing this question requires a framework that treats fractionalization and crystallization on equal footing, especially in strong Landau-level mixing regime. Here, we introduce MagNet, a self-attention neural-network variational wavefunction designed for quantum systems in magnetic fields on the torus geometry. We show that MagNet provides a *unifying* and expressive ansatz capable of describing both FQH states and electron crystals within the same architecture. Trained solely by energy minimization of the microscopic Hamiltonian, MagNet discovers topological liquid and electron crystal ground states across a broad range of Landau-level mixing. Our results highlight the power of first-principles artificial intelligence (AI) for solving strongly interacting many-body problems and finding competing phases without external training data or physics preknowledge.

DOI: 10.1103/9qlr-jp6x

## I. INTRODUCTION

When does a fractional quantum Hall (FQH) liquid crystallize? This question lies at the heart of the competition between topological order and charge ordering in two-dimensional electron systems and has motivated numerous theoretical and numerical efforts [1–6]. It is also directly relevant experimentally [7–11]: by tuning the carrier density and magnetic field, experiments can access both FQH and Wigner crystal regimes in high-mobility two-dimensional semiconductors [12]. Addressing the competition between fractionalization and crystallization in an unbiased manner remains an outstanding challenge, because an interacting two-dimensional electron gas in a magnetic field features an infinite ladder of Landau levels (LLs) and strong electron correlation. Quantum Monte Carlo faces severe complex phase problem, and density matrix renormalization group suffers from discretization errors due to Landau-level truncation. As a result, much of our understanding relies on trial wavefunctions that are tailor-made for FQH liquids and Wigner crystals separately, making it difficult to determine the phase boundary in an unbiased way.

In recent years, neural-network (NN) quantum states [13–15] have emerged as a powerful class of variational wavefunctions and have attained accurate results in continuum Fermi systems [16–19]. Here, the networks are trained directly by minimizing the variational energy of the microscopic Hamiltonian. Remarkably, recent studies [20–24] have found that ground states of vastly different quantum phases—ranging from Fermi liquids and Wigner crystals to fractional Hall states and superconductors—can all be captured within a single neural architecture; fundamentally distinct quantum states simply correspond to different values of network parameters.

This unprecedented expressive power has further motivated the development of *universal* Fermi networks that are provably capable of representing any fermionic wavefunction at sufficient network size [25]. Recently, a universal architecture—"Fermi Sets"—has been introduced [26], which is mathematically proven to achieve universal approximation of continuous fermionic wavefunctions while retaining physical interpretability. Universal Fermi networks of sufficiently large size can in principle solve many-electron Schrodinger equations to arbitrary accuracy. This opens vast opportunities for *first-principles AI* in quantum chemistry, condensed matter physics, material science, and quantum computing.

In this work, we develop a self-attention Fermi network (MagNet) to solve the strongly correlated problem of two-dimensional interacting electrons in a magnetic field, where fractionalization competes with crystallization. In contrast to previous neural-network variational studies [20,27], we work on the torus geometry, which is free of boundary effects and naturally accommodates both topological fluids and crystalline order in an unbiased way. A key innovation is our construction of a real-space neural wavefunction that exactly respects the nontrivial boundary conditions imposed by magnetic translations while remaining extremely expressive. In particular, our network allows for general, intricate phase structures far beyond those of standard quantum Hall model wavefunctions.

Using this unifying architecture, we obtain accurate ground-state energies and wavefunctions across the entire range of Landau-level mixing, from weak to strong. The same neural network discovers both FQH liquids and electron crystals directly from the microscopic Hamiltonian, without

[*]Contact author: ahmed95@mit.edu
[†]Contact author: liangfu@mit.edu

*Published by the American Physical Society under the terms of the Creative Commons Attribution 4.0 International license. Further distribution of this work must maintain attribution to the author(s) and the published article's title, journal citation, and DOI.*

being supplied with any physics knowledge, such as Landau levels, Laughlin states, flux attachment, or crystalline order. All information about fractionalization and crystallization is extracted *a posteriori* from the wavefunction learned by the network through energy minimization alone. In this sense, our work realizes a genuinely first-principles AI solver for this paradigmatic strongly correlated problem.

Beyond verifying known phases in the limit of weak and strong LL mixing, our work provides, for the first time, a unified solution across the FQH-to-crystal topological quantum phase transition, within a single family of variational wavefunctions. This enables us to follow the evolution of correlation functions and structure factors and locate the onset of crystalline order.

More broadly, our study highlights the power of first-principles AI as a general-purpose tool for quantum matter, capable of exploring phase diagrams, discovering unexpected correlated phases, and offering microscopic insights into the organizing principles of strongly interacting electrons.

## II. SETUP

Our starting point is the standard problem of two-dimensional electrons subject to an external magnetic field and interacting with Coulomb potential. The many-body Hamiltonian of $N$ particles reads

$$H = \sum_i \frac{(-i\hbar\nabla_i + e\boldsymbol{A}(\boldsymbol{r}_i))^2}{2m} + \frac{1}{2}\sum_{i\neq j}\frac{e^2}{4\pi\epsilon|\boldsymbol{r}_i - \boldsymbol{r}_j|}, \quad (1)$$

where $\boldsymbol{A}(\boldsymbol{r})$ is the vector potential of the magnetic field $\boldsymbol{B} = \nabla \times \boldsymbol{A}(\boldsymbol{r})$. This problem is governed by two energy scales, the kinetic energy scale $K = \hbar\omega_c$ that sets the gap between the (infinite) ladder of flat Landau levels with $\omega_c = eB/m$ the cyclotron frequency and interaction scale $U = e^2/4\pi\epsilon\ell_B$ that sets the strength of the Coulomb repulsion in terms of the magnetic length $\ell_B = \sqrt{\hbar/eB}$. The many-body ground state at filling factor $\nu$ is therefore controlled by the ratio of the two, $\kappa = U/K \propto 1/\sqrt{B}$, which describes the amount of Landau-level mixing. $\kappa$ is related to the dimensionless interaction strength parameter $r_s = 1/\sqrt{\pi a_B^2 n}$ through $\kappa = r_s\sqrt{\nu/2}$, where $a_B = \hbar^2/e^2m$ is the Bohr radius and $n$ is the density. Experimentally, for a given magnetic field, $\kappa$ is material dependent and can become very large in materials with heavy effective mass, such as hole-doped GaAs, ZnO, or transition-metal dichalcogenides [9,12,28–31].

Focusing on $\nu < 1$, the physics in the limit $\kappa \to 0$ is confined to the lowest Landau level where fractional quantum Hall liquids arise at various fillings, while increasing $\kappa$ drives substantial Landau-level mixing and can quantitatively change the ground state. In particular, when $\kappa \to \infty$, interactions dominate over kinetic energy and the ground state becomes a classical Wigner crystal. At intermediate values of $\kappa$, the system lies in a genuinely nonperturbative regime, and the FQH liquid competes with various possible charge-ordered states such as Wigner crystals, composite-fermion crystals [2,32–36], or Hall crystals [37]. Resolving this competition requires a method that can treat strong Landau-level mixing, while remaining unbiased with respect to competing states.

To proceed, we work on the torus geometry that is defined by two basis vectors $\boldsymbol{L}_1$ and $\boldsymbol{L}_2$, and is pierced by a magnetic field whose total flux is quantized to an integer number $N_\phi$ of flux quanta, fixed by $|\boldsymbol{L}_1 \times \boldsymbol{L}_2| = 2\pi N_\phi \ell_B^2$. The torus provides a particularly favorable geometry for studying competing quantum phases. Unlike the disk, it has no physical edge and therefore avoids boundary effects and edge reconstruction [38]. Compared to the sphere, it also avoids curvature and the associated topological shift [39] that can complicate finite-size comparisons across different phases. Additionally, the torus naturally accommodates translational symmetry, making it well suited not only for uniform quantum Hall liquids but also for charge-ordered phases such as Wigner crystals, whose periodicity can be embedded commensurately in the torus supercell.

## III. MAGNET

To comply with the periodicity of the torus, any wavefunction has to transform under translation of a single particle as [40]

$$\Psi(\boldsymbol{r}_1, \ldots, \boldsymbol{r}_i + \boldsymbol{L}, \ldots, \boldsymbol{r}_N) = e^{i\varphi}e^{i\xi_{\boldsymbol{L}}(\boldsymbol{r}_i)}\Psi(\boldsymbol{r}_1, \ldots, \boldsymbol{r}_N), \quad (2)$$

where $\xi_{\boldsymbol{L}}(\boldsymbol{r}_i)$ is the magnetic phase determined by $\nabla\xi_{\boldsymbol{L}}(\boldsymbol{r}_i) = \frac{e}{\hbar}[\boldsymbol{A}(\boldsymbol{r}_i + \boldsymbol{L}) - \boldsymbol{A}(\boldsymbol{r}_i)]$ and $\boldsymbol{L} = m\boldsymbol{L}_1 + n\boldsymbol{L}_2$ is a generic torus vector with integers $m$ and $n$. $\varphi$ is an additional twist phase corresponding to threading flux through the handles of the torus, implemented by a constant vector potential.

Importantly, condition (2) implies that the net winding $\mathcal{W}$ of the wavefunction as a function of one particle coordinate $\boldsymbol{r}_i$ (while fixing the remaining $N-1$ particles $\{\boldsymbol{r}_{\neq i}\}$) has to be $\mathcal{W} = N_\phi$ [41,42]. This net winding constraint requires the wavefunction to contain phase singularities on the torus—i.e., vortices where $\Psi$ vanishes and its phase winds. In general, the wavefunction may host both vortices and antivortices, but their contributions must sum to the same net winding: the total winding (vortices counted with positive charge minus antivortices counted with negative charge) is fixed to $N_\phi$.

Our variational wavefunction for the many-body ground state is given by

$$\Psi_{\{\theta\}}(\{\boldsymbol{r}_i\}) = e^{\mathcal{J}(\{\boldsymbol{r}_i\})}\sum_n^{N_{\text{det}}}\det\left[\phi_j^n(\boldsymbol{r}_i;\{\boldsymbol{r}_{\neq i}\})\right], \quad (3)$$

where $\phi_j^n(\boldsymbol{r}_i;\{\boldsymbol{r}_{\neq i}\})$ is a generalized many-body orbital for the $i$th particle that depends on the coordinates of the remaining particles $\boldsymbol{r}_{\neq i}$. $\{\theta\}$ denotes the variational parameters of the ansatz. $\mathcal{J}(\{\boldsymbol{r}_i\})$ is a periodic symmetric Jastrow factor, $\mathcal{J}(\boldsymbol{r}_1, \ldots, \boldsymbol{r}_i + \boldsymbol{L}, \ldots, \boldsymbol{r}_N) = \mathcal{J}(\boldsymbol{r}_1, \ldots, \boldsymbol{r}_N)$, to enforce electron cusp conditions for long-range Coulomb interactions. However, the existence of a Jastrow factor here is not generally needed and we obtained similar results without it.

To respect fermionic antisymmetry, $\phi_j^n$ has to be permutation *invariant* in the coordinates $\{\boldsymbol{r}_{\neq i}\}$ [14,21]. Moreover, to enforce magnetic boundary condition (2), $\phi_j^n$ transforms under translations of $\boldsymbol{r}_i$ as

$$\phi_j^n(\boldsymbol{r}_i + \boldsymbol{L}, \{\boldsymbol{r}_{\neq i}\}) = e^{i\varphi}e^{i\xi_{\boldsymbol{L}}(\boldsymbol{r}_i)}\phi_j^n(\boldsymbol{r}_i;\{\boldsymbol{r}_{\neq i}\}) \quad (4)$$

and is periodic in the rest $\{\boldsymbol{r}_{\neq i}\}$:

$$\phi_j^n(\boldsymbol{r}_i, \{\ldots, \boldsymbol{r}_k + \boldsymbol{L}, \ldots, \boldsymbol{r}_l, \ldots\}) = \phi_j^n(\boldsymbol{r}_i;\{\boldsymbol{r}_{\neq i}\}) \quad (5)$$

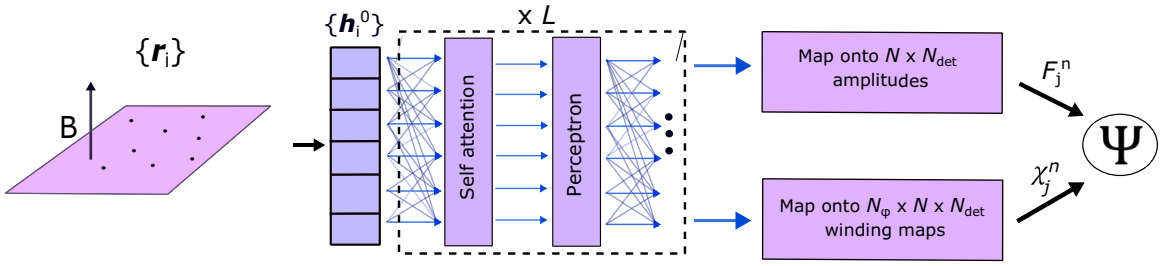



FIG. 1. Schematic illustration of the MagNet architecture: Electron coordinates (in the presence of magnetic field) are mapped to higher-dimensional feature space that is passed to $L$ layers of successive self-attention and multilayer perceptron blocks. The final output undergoes two different mappings to form the generalized orbitals (6) that build the full variational ansatz. For simplicity, we show a plane pierced by a magnetic field but our ansatz is designed for the torus geometry.

for $k, l, \ldots \neq i$. A sum of determinants over $\phi_j^n$ as in ansatz (3) automatically satisfies condition (2) and therefore represents a physically valid wavefunction on the torus.

Furthermore, $\phi_j^n$ is factorized into a product,

$$\phi_j^n(\boldsymbol{r}_i; \{\boldsymbol{r}_{\neq i}\}) = \chi_j^n(\boldsymbol{r}_i; \{\boldsymbol{r}_{\neq i}\}) F_j^n(\boldsymbol{r}_i; \{\boldsymbol{r}_{\neq i}\}), \tag{6}$$

where $F_j^n$ is a periodic function in all coordinates, $F_j^n(\boldsymbol{r}_1, \ldots, \boldsymbol{r}_i + \boldsymbol{L}, \boldsymbol{r}_N) = F_j^n(\boldsymbol{r}_1, \ldots, \boldsymbol{r}_N)$, while $\chi_j^n$ transforms similar to $\phi_j^n$ [Eqs. (4) and (5)].

To impose a net winding of $N_\phi$, the core innovation of our ansatz is to parametrize $\chi_j^n$ in terms of a product over $N_\phi$ terms,

$$\chi_j^n(\boldsymbol{r}_i; \{\boldsymbol{r}_{\neq i}\}) = \prod_{\alpha=1}^{N_\phi} f\big(z_i - \eta_j^{(n,\alpha)}(\{\boldsymbol{r}\})\big), \tag{7}$$

where $f(z_i)$ is a gauge-dependent quasiperiodic function in the coordinate $z_i$ with net winding $\mathcal{W} = +1$ in the fundamental domain of the torus spanned by $\boldsymbol{L}_1$ and $\boldsymbol{L}_2$, and $z_i = x_i + iy_i$ is the complex coordinate of $\boldsymbol{r}_i$. For our purposes, the function $f(z_i - \eta)$ vanishes when $z_i = \eta$. Importantly, $\eta_j^{(n,\alpha)}(\{\boldsymbol{r}\})$ here is a *learnable* periodic and symmetric many-body function in *all* coordinates. The zeros of $\chi_j^n$ and their windings are determined through the solutions of $z_i = \eta_j^{(n,\alpha)}(\{\boldsymbol{r}\})$. For this reason, we refer to $\eta_j^{(n,\alpha)}(\{\boldsymbol{r}\})$ as a winding map.

We note that if the winding maps $\{\eta\}$ in Eq. (7) are taken to be fixed parameters (no dependence on $\{\boldsymbol{r}\}$), then $\chi_j^n$ reduces to the single-particle lowest-Landau-level (LLL) wavefunction that is specified by $N_\phi$ vortices and is holomorphic (up to a Gaussian factor) [41,43]. In contrast, allowing $\{\eta\}$ to depend on all particle coordinates—including $\boldsymbol{r}_i$ itself—generically introduces $\bar{z}$ dependence, so that $\chi_j^n$ becomes nonholomorphic. Together with the additional periodic factor $F_j^n$, this nonholomorphic structure enables the full many-body ansatz to represent states residing outside the LLL. Crucially, by promoting the zeros of the generalized orbitals to be many-body trainable functions, the variational ansatz can capture nontrivial phase effects in a correlated manner. To proceed, we work in the symmetric gauge, $A(\boldsymbol{r}) = B_0(\hat{z} \times \boldsymbol{r})/2$, where $B_0$ denotes the uniform component of the magnetic field. In this gauge, the magnetic translation phase takes the form

$$e^{i\xi_L(\boldsymbol{r})} = (-1)^{N_\phi(mn+m+n)} e^{i(\boldsymbol{r}\times\boldsymbol{L})/2\ell_B^2} \tag{8}$$

for $\boldsymbol{L} = m\boldsymbol{L}_1 + n\boldsymbol{L}_2$. We choose $f(z)$ in Eq. (7) to be the modified Weierstrass sigma function [44–46]. In this representation, the sum of the winding maps, $\overline{\eta}_j^{(n)} = (\sum_\alpha \eta_j^{(n,\alpha)}) \bmod (L_x + iL_y)$, fixes the twist phase $\varphi$ in Eq. (4). Throughout, we set $\varphi = 0$ by imposing the constraint $\overline{\eta}_j^{(n)} = 0$ [40].

Next, we represent the generalized orbitals $\phi_j^n$ with a deep neural network (Fig. 1) based on the self-attention mechanism [21,47]. As initial input, the NN takes the *periodized* coordinates of the particles on the torus [$\sin(\boldsymbol{G}_a \cdot \boldsymbol{r}_i)$ and $\cos(\boldsymbol{G}_a \cdot \boldsymbol{r}_i)$], where $\boldsymbol{G}_{a=1,2}$ are the reciprocal lattice vectors, i.e., $\boldsymbol{G}_a \cdot \boldsymbol{L}_b = 2\pi\delta_{ab}$. These inputs are then passed through $L$ layers of successive self-attention and perceptron blocks. The final output of the NN is mapped to construct the amplitudes $F_j^n$ and the winding maps $\eta_j^{(n,\alpha)}$ of $\chi_j^n$ to form the generalized orbitals $\phi_j^n$. The parameters of the ansatz $\{\theta\}$ are optimized through energy minimization to yield the final ansatz (3). Our construction is distinct from very recent work [48] in several key aspects. Rather than a linear combination of single-particle orbitals, the quasiperiodic function $\chi_j^n$ (7) is parametrized by its zeros, as determined by winding maps $\{\eta\}$ that depend on *all* particle coordinates, leading to enhanced expressivity. Moreover, as we shall demonstrate below, our parametrization successfully captures fractional quantum Hall liquids without additional neural-network Jastrow factor. We refer the reader to the Supplemental Material [40] for comprehensive details about the architecture and the optimization.

## IV. RESULTS

To test the validity of our ansatz, we apply it to the Hamiltonian (1) at filling factor $\nu = 1/3$. At $\kappa = 3.0$, the optimized neural-network wavefunction exhibits hallmarks of a fractional quantum Hall liquid. Figure 2(a) shows the pair-correlation function $g(\boldsymbol{r}) = \frac{A}{N^2}\langle\sum_{i\neq j}\delta^2(\boldsymbol{r} - \boldsymbol{r}_i + \boldsymbol{r}_j)\rangle$ and Fig. 2(b) shows the structure factor $S(\boldsymbol{q}) = \frac{1}{N}\langle\rho_{\boldsymbol{q}}\rho_{-\boldsymbol{q}}\rangle$, with the density operator $\rho_{\boldsymbol{q}} = \sum_i e^{i\boldsymbol{q}\cdot\boldsymbol{r}_i}$. In both cases, the density correlations in the ground state are liquidlike, indicating the absence of crystalline order in the ground state.

Next, we probe the existence of topological order by demonstrating the expected topological ground-state degeneracy [24]. To this end, we decompose the optimized many-body wavefunction $\Psi(\{\boldsymbol{r}\})$ onto center-of-mass (CM) momentum sectors $\Phi_K(\{\boldsymbol{r}\})$, defined as eigenstates of the CM magnetic

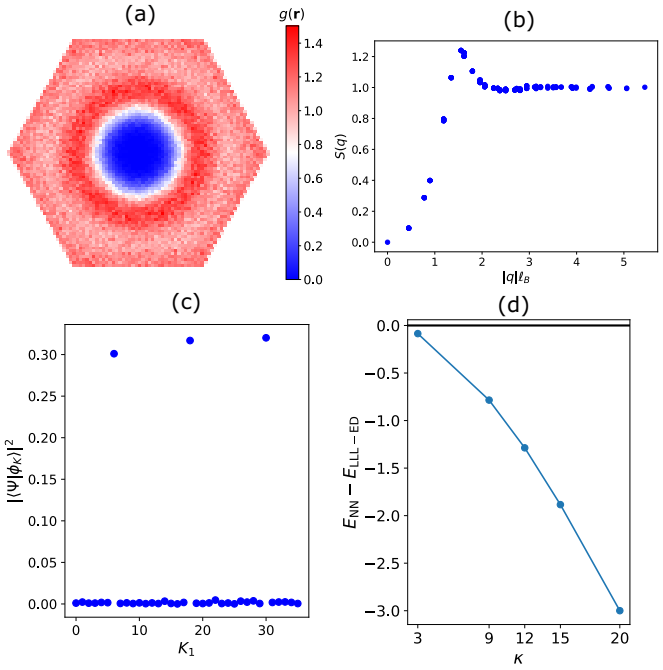



FIG. 2. (a) Pair-correlation function $g(\boldsymbol{r})$ at $\kappa = 3.0$. (b) The structure factor $S(\boldsymbol{q})$ along a line cut at $\kappa = 3.0$. (c) The overlap $|\langle\Psi|\Phi_{K_1}\rangle|^2$ of the optimized wavefunction $\Psi$ at $\kappa = 3.0$ with its projection $\Phi_{K_1}$ defined as the eigenstates of CM magnetic translation operator along $L_1$. (d) Comparison of the variational energy of the NN ansatz $E_{\mathrm{NN}}$ (in units of $\hbar\omega_c$) against the energies obtained from exact diagonalization $E_{\mathrm{LLL\text{-}ED}}$ projected onto the lowest Landau level for various values of $\kappa$. All calculations are performed at filling $\nu = 1/3$ ($N = 12$ and $N_\phi = 36$) on a hexagonal torus with equal aspect ratio.

translation operator $T_{\mathrm{CM}}(n\boldsymbol{L}_1/N_\phi)$, with $n = 0, \ldots, N_\phi - 1$. As shown in Fig. 2(c), the resulting state carries nonzero weight in only three CM momentum sectors, matching precisely the sectors of the $\nu = 1/3$ Laughlin state for the same finite-size geometry. Taken together, our findings establish the ability of the NN ansatz to discover a fractional quantum Hall liquid on the torus geometry.

To further corroborate the effectiveness of our ansatz in capturing strong Landau-level mixing, we compare its energy against LLL) projected exact diagonalization (ED) in Fig. 2(d). We find that the NN achieves consistently lower variational energies than the corresponding ED energies. This highlights a key advantage of our approach: For this system size ($N_\phi = 36$), ED is restricted to the LLL and can only capture an FQH liquid regardless of $\kappa$, whereas our real-space NN ansatz naturally incorporates Landau-level mixing without truncation and allows for competing phases.

To address whether strong Landau-level mixing can destabilize the fractional quantum Hall liquid, we use our unified NN ansatz to study the evolution of the many-body ground state as a function of $\kappa$. As shown in Figs. 3(a)–3(c), the pair-correlation function $g(\boldsymbol{r})$ evolves from being featureless and liquidlike to exhibiting well-developed spatial modulations as $\kappa$ increases, signaling a transition toward a crystalline phase.

To assess whether these correlations correspond to true long-range crystalline order in the thermodynamic limit, we perform a finite-size scaling of the structure factor $S(\boldsymbol{q})$. First, we find $S(\boldsymbol{q})$ to have maximum value at $\boldsymbol{q} = \boldsymbol{K}$ for various values of $\kappa$, with $\boldsymbol{K}$ being the ordering wave vector of a crystal with one electron per unit cell. However, as shown in Fig. 3(d), the magnitude of this peak $S(\boldsymbol{K})$ exhibits only a small enhancement with increasing particle number $N$ for $\kappa = 12$ and $\kappa = 15$, suggesting at most incipient charge order at these values. In contrast, for $\kappa = 20$ we find that $S(\boldsymbol{K})$ grows approximately linearly with $N$, consistent with the development of true long-range crystalline order. On the other hand, for $\kappa = 3$, $S(\boldsymbol{K})$ does not grow with $N$ and is nearly constant, consistent with an FQH liquid.

The robustness of the Laughlin liquid at $\nu = 1/3$ against crystallization for strong Landau-level mixing is rather special, as can be seen by contrasting it with nearby fillings. As shown in Fig. 4, at the same value of Landau-level mixing for which the $\nu = 1/3$ ground state remains a homogeneous liquid [Fig. 4(a)], a slight doping away from this commensurate filling, to $\nu = 0.3$, already favors a crystalline ground state [Fig. 4(b)]. This is further supported by the finite-size scaling of the structure factor shown in Fig. 4(c). The existence of crystallization in the vicinity of the FQH liquid is consistent with experimental results [7–10].

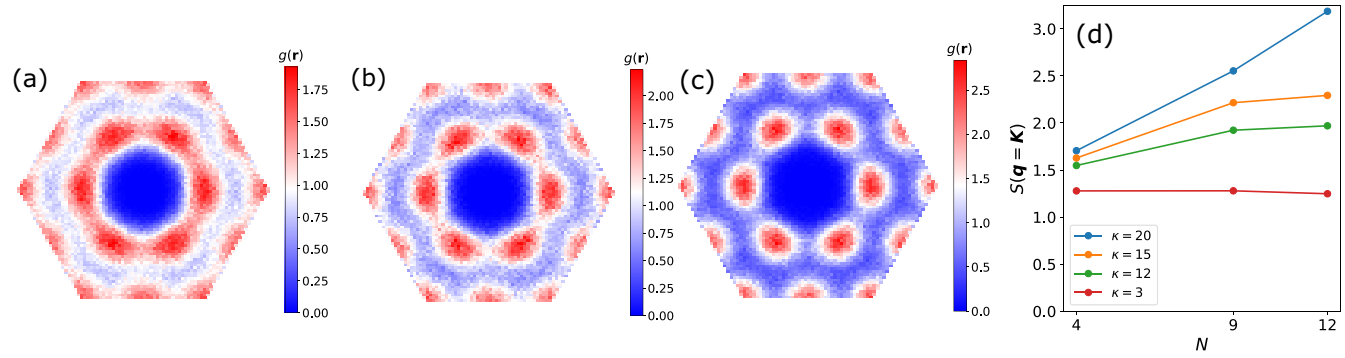



FIG. 3. Pair-correlation function $g(\boldsymbol{r})$ at $\nu = 1/3$ for (a) $\kappa = 12$, (b) $\kappa = 15$, and (c) $\kappa = 20$. (d) Structure factor $S(\boldsymbol{q})$ evaluated at the ordering wave vector $\boldsymbol{q} = \boldsymbol{K}$ corresponding to a crystal with one electron per unit cell, plotted as a function of particle number $N$ for various values of $\kappa$. The reported $S(\boldsymbol{q} = \boldsymbol{K})$ is rotationally averaged over the six $C_6$-related ordering wave vectors. All calculations are performed with $N = 12$ and $N_\phi = 36$ on a hexagonal torus with equal aspect ratio.

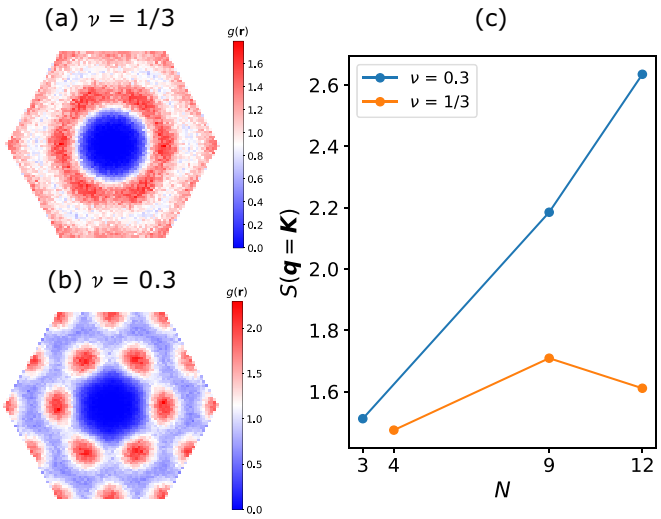



FIG. 4. Pair-correlation function $g(\boldsymbol{r})$ at $\kappa = 9$ for (a) $\nu = 1/3$ and (b) $\nu = 0.3$. (c) Structure factor $S(\boldsymbol{q})$ evaluated at the ordering wave vector $\boldsymbol{q} = \boldsymbol{K}$ corresponding to a crystal with one electron per unit cell as a function of number of particles $N$ at $\kappa = 9$. Calculations in panels (a) and (b) are performed with $N = 12$ on a hexagonal torus enclosing $N_\phi = 36$ and $N_\phi = 40$.

## V. DISCUSSION

In this paper, we have introduced MagNet, a self-attention neural-network variational wavefunction to study quantum systems subject to magnetic fields on the torus geometry. We have shown that MagNet captures both fractional quantum Hall liquids and crystals in a unified manner. While we have presented evidence of pronounced crystalline correlations with increasing Landau-level mixing, the full nature of the crystal phase is yet to be established. Apart from topologically trivial Wigner crystal or the composite-fermion crystal, an intriguing possibility is the realization of (integer or fractional) Hall crystal [37,49–51], a state that spontaneously breaks magnetic translational symmetry but has quantized Hall conductance.

Earlier numerical work [3] suggested that the $\nu = 1/3$ FQH liquid undergoes a transition to a crystalline phase at Landau-level mixing, around $\kappa \approx 9$ (corresponding to $r_s \approx 22$). In contrast, more recent studies based on fixed-phase diffusion Monte Carlo [2]—where the complex phase of the trial state is constrained to be that of a composite-fermion wavefunction—did not find crystallization of the $\nu = 1/3$ FQH liquid up to the largest mixing strength considered, $\kappa = 18$ ($r_s \approx 44$). In comparison with these results, our unbiased variational Monte Carlo results—obtained within a single unified ansatz and based on the system sizes accessible here—indicate that long-range crystalline order emerges between $\kappa = 15$ ($r_s \approx 37$) and $\kappa = 20$ ($r_s \approx 49$) (cf. Fig. 4).

The development of a neural-network ansatz that can treat arbitrary Landau-level mixing opens a powerful route to studying a wide range of quantum Hall problems in an unbiased, first-principles manner. While we have focused on $\nu = 1/3$, a natural next step is to apply this framework across a broader set of filling factors to investigate the competition between liquid phases—including incompressible FQH states and compressible composite-fermion Fermi liquids—and crystalline order.

Finally, our neural-network ansatz is naturally suited to problems with spatially nonuniform magnetic fields or external modulations [52], such as moiré systems—for example, twisted TMDs—where the moiré potential generates emergent spatially modulated magnetic fields [53–55].

## ACKNOWLEDGMENTS

We are grateful to Aidan Reddy, Timothy Zaklama, and Filippo Gaggioli for useful discussions and related collaborations. We thank Timothy Zaklama for coining the NN architecture name and acknowledge insightful discussions with Max Geier, Daniele Guerci, and Pierre-Antoine Graham. This work was supported by a Simons Investigator Award from the Simons Foundation. A.A. was supported by the Knut and Alice Wallenberg Foundation (KAW 2022.0348). This work made use of resources provided by subMIT at MIT Physics. The authors acknowledge the MIT Office of Research Computing and Data for providing high-performance computing resources that have contributed to the research results reported within this paper.

## DATA AVAILABILITY

The data that support the findings of this article are not publicly available. The data are available from the authors upon reasonable request.

[1] G. Ortiz, D. Ceperley, and R. Martin, New stochastic method for systems with broken time-reversal symmetry: 2D fermions in a magnetic field, Phys. Rev. Lett. **71**, 2777 (1993).

[2] J. Zhao, Y. Zhang, and J. Jain, Crystallization in the fractional quantum Hall regime induced by Landau-level mixing, Phys. Rev. Lett. **121**, 116802 (2018).

[3] R. Price, P. Platzman, and S. He, Fractional quantum Hall liquid, Wigner solid phase boundary at finite density and magnetic field, Phys. Rev. Lett. **70**, 339 (1993).

[4] P. Platzman and R. Price, Quantum freezing of the fractional quantum Hall liquid, Phys. Rev. Lett. **70**, 3487 (1993).

[5] X. Zhu and S. G. Louie, Wigner crystallization in the fractional quantum Hall regime: A variational quantum Monte Carlo study, Phys. Rev. Lett. **70**, 335 (1993).

[6] W. He, T. Cui, Y. Ma, C. Chen, Z. Liu, and G. Zou, Phase boundary between the fractional quantum Hall liquid and the Wigner crystal at low filling factors and low temperatures: A path integral Monte Carlo study, Phys. Rev. B **72**, 195306 (2005).

[7] M. Santos, Y. Suen, M. Shayegan, Y. Li, L. Engel, and D. Tsui, Observation of a reentrant insulating phase near the 1/3 fractional quantum Hall liquid in a two-dimensional hole system, Phys. Rev. Lett. **68**, 1188 (1992).

[8] M. Santos, J. Jo, Y. Suen, L. Engel, and M. Shayegan, Effect of Landau-level mixing on quantum-liquid and solid states of two-dimensional hole systems, Phys. Rev. B **46**, 13639 (1992).

[9] D. Maryenko, A. McCollam, J. Falson, Y. Kozuka, J. Bruin, U. Zeitler, and M. Kawasaki, Composite fermion liquid to Wigner solid transition in the lowest Landau level of zinc oxide, Nat. Commun. **9**, 4356 (2018).

[10] W. Pan, G. Csáthy, D. Tsui, L. Pfeiffer, and K. West, Transition from a fractional quantum Hall liquid to an electron solid at Landau level filling $\nu = 1/3$ in tilted magnetic fields, Phys. Rev. B **71**, 035302 (2005).

[11] Y.-C. Tsui, M. He, Y. Hu, E. Lake, T. Wang, K. Watanabe, T. Taniguchi, M. P. Zaletel, and A. Yazdani, Direct observation of a magnetic-field-induced Wigner crystal, Nature (London) **628**, 287 (2024).

[12] J. Pack, Y. Guo, Z. Liu, B. S. Jessen, L. Holtzman, S. Liu, M. Cothrine, K. Watanabe, T. Taniguchi, D. G. Mandrus, *et al.*, Charge-transfer contacts for the measurement of correlated states in high-mobility $WSe_2$, Nat. Nanotechnol. **19**, 948 (2024).

[13] G. Carleo and M. Troyer, Solving the quantum many-body problem with artificial neural networks, Science **355**, 602 (2017).

[14] D. Pfau, J. S. Spencer, A. G. Matthews, and W. M. C. Foulkes, *Ab initio* solution of the many-electron Schrödinger equation with deep neural networks, Phys. Rev. Res. **2**, 033429 (2020).

[15] D. Luo and B. K. Clark, Backflow transformations via neural networks for quantum many-body wave functions, Phys. Rev. Lett. **122**, 226401 (2019).

[16] G. Cassella, H. Sutterud, S. Azadi, N. D. Drummond, D. Pfau, J. S. Spencer, and W. M. C. Foulkes, Discovering quantum phase transitions with fermionic neural networks, Phys. Rev. Lett. **130**, 036401 (2023).

[17] C. Smith, Y. Chen, R. Levy, Y. Yang, M. A. Morales, and S. Zhang, Unified variational approach description of ground-state phases of the two-dimensional electron gas, Phys. Rev. Lett. **133**, 266504 (2024).

[18] G. Pescia, J. Nys, J. Kim, A. Lovato, and G. Carleo, Message-passing neural quantum states for the homogeneous electron gas, Phys. Rev. B **110**, 035108 (2024).

[19] D. Luo, D. D. Dai, and L. Fu, Pairing-based graph neural network for simulating quantum materials, arXiv:2311.02143.

[20] Y. Teng, D. D. Dai, and L. Fu, Solving the fractional quantum Hall problem with self-attention neural network, Phys. Rev. B **111**, 205117 (2025).

[21] M. Geier, K. Nazaryan, T. Zaklama, and L. Fu, Self-attention neural network for solving correlated electron problems in solids, Phys. Rev. B **112**, 045119 (2025).

[22] C.-T. Li, T. Ong, M. Geier, H. Lin, and L. Fu, Attention is all you need to solve chiral superconductivity, arXiv:2509.03683.

[23] K. Nazaryan, F. Gaggioli, Y. Teng, and L. Fu, Artificial intelligence for quantum matter: Finding a needle in a haystack, arXiv:2507.13322.

[24] A. Abouelkomsan, M. Geier, and L. Fu, Topological order in deep state, Phys. Rev. B **113**, 205119 (2026).

[25] L. Fu, A minimal and universal representation of fermionic wavefunctions (fermions = bosons + one), arXiv:2510.11431.

[26] L. Fu, Fermi sets: Universal and interpretable neural architectures for fermions, arXiv:2601.02508.

[27] Y. Qian, T. Zhao, J. Zhang, T. Xiang, X. Li, and J. Chen, Describing Landau level mixing in fractional quantum Hall states with deep learning, Phys. Rev. Lett. **134**, 176503 (2025).

[28] I. Sodemann and A. MacDonald, Landau level mixing and the fractional quantum Hall effect, Phys. Rev. B **87**, 245425 (2013).

[29] C. Wang, A. Gupta, P. T. Madathil, S. K. Singh, Y. J. Chung, L. N. Pfeiffer, K. W. Baldwin, and M. Shayegan, Next-generation even-denominator fractional quantum Hall states of interacting composite fermions, Proc. Natl. Acad. Sci. USA **120**, e2314212120 (2023).

[30] A. Tsukazaki, S. Akasaka, K. Nakahara, Y. Ohno, H. Ohno, D. Maryenko, A. Ohtomo, and M. Kawasaki, Observation of the fractional quantum Hall effect in an oxide, Nat. Mater. **9**, 889 (2010).

[31] Q. Shi, E.-M. Shih, M. V. Gustafsson, D. A. Rhodes, B. Kim, K. Watanabe, T. Taniguchi, Z. Papić, J. Hone, and C. R. Dean, Odd- and even-denominator fractional quantum Hall states in monolayer $WSe_2$, Nat. Nanotechnol. **15**, 569 (2020).

[32] A. C. Archer and J. K. Jain, Static and dynamic properties of type-II composite fermion Wigner crystals, Phys. Rev. B **84**, 115139 (2011).

[33] H. Yi and H. Fertig, Laughlin-Jastrow-correlated Wigner crystal in a strong magnetic field, Phys. Rev. B **58**, 4019 (1998).

[34] R. Narevich, G. Murthy, and H. Fertig, Hamiltonian theory of the composite-fermion Wigner crystal, Phys. Rev. B **64**, 245326 (2001).

[35] C.-C. Chang, G. S. Jeon, and J. K. Jain, Microscopic verification of topological electron-vortex binding in the lowest Landau-level crystal state, Phys. Rev. Lett. **94**, 016809 (2005).

[36] A. C. Archer, K. Park, and J. K. Jain, Competing crystal phases in the lowest Landau level, Phys. Rev. Lett. **111**, 146804 (2013).

[37] Z. Tesanovic, F. Axel, and B. Halperin, "hall crystal" versus wigner crystal, Phys. Rev. B **39**, 8525 (1989).

[38] X. Wan, E. Rezayi, and K. Yang, Edge reconstruction in the fractional quantum Hall regime, Phys. Rev. B **68**, 125307 (2003).

[39] X.-G. Wen and A. Zee, Shift and spin vector: New topological quantum numbers for the Hall fluids, Phys. Rev. Lett. **69**, 953 (1992).

[40] See Supplemental Material at https://link.aps.org/supplemental/10.1103/9qlr-jp6x for additional details.

[41] F. D. M. Haldane, Many-particle translational symmetries of two-dimensional electrons at rational Landau-level filling, Phys. Rev. Lett. **55**, 2095 (1985).

[42] F. D. M. Haldane and E. H. Rezayi, Periodic Laughlin-Jastrow wave functions for the fractional quantized Hall effect, Phys. Rev. B **31**, 2529 (1985).

[43] M. Fremling, Coherent state wave functions on a torus with a constant magnetic field, J. Phys. A: Math. Theor. **46**, 275302 (2013).

[44] F. Haldane, A modular-invariant modified Weierstrass sigma-function as a building block for lowest-Landau-level wavefunctions on the torus, J. Math. Phys. **59**, 071901 (2018).

[45] F. Haldane, The origin of holomorphic states in Landau levels from non-commutative geometry and a new formula for their overlaps on the torus, J. Math. Phys. **59**, 081901 (2018).

[46] J. Wang, S. D. Geraedts, E. Rezayi, and F. Haldane, Lattice Monte Carlo for quantum Hall states on a torus, Phys. Rev. B **99**, 125123 (2019).

[47] I. von Glehn, J. S. Spencer, and D. Pfau, A self-attention ansatz for *ab-initio* quantum chemistry, arXiv:2211.13672.

[48] A. P. Fadon, D. Pfau, J. S. Spencer, W. T. Lou, T. Neupert, and W. Foulkes, Extracting anyon statistics from neural network fractional quantum Hall states, arXiv:2512.15872.

[49] B. Halperin, Z. Tesanovic, and F. Axel, Compatibility of crystalline order and the quantized Hall effect, Phys. Rev. Lett. **57**, 922 (1986).

[50] G. Murthy, Hall crystal states at $\nu = 2$ and moderate Landau level mixing, Phys. Rev. Lett. **85**, 1954 (2000).

[51] S. Kivelson, C. Kallin, D. P. Arovas, and J. R. Schrieffer, Cooperative ring exchange theory of the fractional quantized Hall effect, Phys. Rev. Lett. **56**, 873 (1986).

[52] N. Paul, Y. Zhang, and L. Fu, Giant proximity exchange and flat Chern band in 2D magnet-semiconductor heterostructures, Sci. Adv. **9**, eabn1401 (2023).

[53] F. Wu, T. Lovorn, E. Tutuc, I. Martin, and A. MacDonald, Topological insulators in twisted transition metal dichalcogenide homobilayers, Phys. Rev. Lett. **122**, 086402 (2019).

[54] N. Morales-Durán, N. Wei, J. Shi, and A. H. MacDonald, Magic angles and fractional Chern insulators in twisted homobilayer transition metal dichalcogenides, Phys. Rev. Lett. **132**, 096602 (2024).

[55] J. Shi, N. Morales-Durán, E. Khalaf, and A. H. MacDonald, Adiabatic approximation and Aharonov-Casher bands in twisted homobilayer transition metal dichalcogenides, Phys. Rev. B **110**, 035130 (2024).